An interactive boundary layer modelling methodology for aerodynamic flows

L. Smith

University of Pretoria
Pretoria, Gauteng, South Africa

O.F. Oxtoby

Aeronautics Systems, Council for Scientific and Industrial Research
Pretoria, Gauteng, South Africa

A.G. Malan

Council for Scientific and Industrial Research
Pretoria, Gauteng, South Africa, and

J.P. Meyer

University of Pretoria
Pretoria, Gauteng, South Africa

Abstract

Purpose – The purpose of this paper is to introduce a unique technique to couple the two-integral boundary layer solutions to a generic inviscid solver in an iterative fashion.

Design/methodology/approach –The boundary layer solution is obtained using the two-integral method to solve displacement thickness point by point with a local Newton method, at a fraction of the cost of a conventional mesh-based, full viscous solution. The boundary layer solution is coupled with an existing inviscid solver. Coupling occurs by moving the wall to a streamline at the computed boundary layer thickness and treating it as a slip boundary, then solving the flow again and iterating. The Goldstein singularity present when solving boundary layer equations is overcome by solving an auxiliary velocity equation along with the displacement thickness.

Findings – The proposed method obtained favourable results when compared with the analytical solutions for flat and inclined plates. Further, it was applied to modelling the flow around a NACA0012 airfoil and yielded results similar to those of the widely used XFOIL code.

Originality/value – A unique method is proposed for coupling of the boundary layer solution to the inviscid flow. Rather than the traditional transpiration boundary condition, mesh movement is employed to simulate the boundary layer thickness in a more physically meaningful way. Further, a new auxiliary velocity equation is presented to circumvent the Goldstein singularity.

Paper type Research paper

Nomenclature

c	Artificial compressibility pseudo-acoustic velocity	$m.s^{-1}$	L	Length	m
			M	Mach number	
c	Chord length	m	$\mathbf{n}$	Unit vector normal to the boundary	
C_D	Dissipation coefficient		N	Maximum number of nodes	
C_f	Skin friction coefficient		p	Pressure	$N.m^{-2}$
d	Original grid position	m	Re	Reynolds number based on L	
f	Body force component	N	Re_θ	Reynolds number based on θ	
h	Height	m	t	Time	
H	Shape factor		u	Velocity component	$m.s^{-1}$
H^*	Energy thickness shape factor		U	Free-stream velocity	$m.s^{-1}$
H^{**}	Density thickness		V	Volume flow rate	$m^3.s$
J	Jacobian		x	Length	m

Greek letters

α	Under-relaxation parameter	
β	Similarity parameter	
$\boldsymbol{\delta}$	Displacement grid position	
δ^*	Boundary layer thickness	m
δ^{**}	Density thickness	
δ_{ij}	Kronecker delta	
Δ	Difference	
η	Similarity coordinate	
θ	Momentum thickness	m
θ^*	Kinetic energy thickness	
μ	Dynamic viscosity	kg.m^{-1}.s^{-1}
ρ	Density	kg.m^{-3}
τ	Shear stress	N.m^{-2}
v	Kinematic viscosity	m^2.s^{-1}
ξ	Coordinate parallel to the boundary layer	m

Subscripts

0	Initial value
$1,2$	Variables in the *x*- and *y*-directions respectively
e	External flow variable
f	Fluid
∞	Free-stream value
i, j, k	Components of vector/tensor in indicial notation
n	Index of nodes along boundary layer
w	Wall

Superscripts

n	pseudo-(iteration) time-step

1. Introduction

Since the 1970s, CFD codes have been used in the aerospace industry to assist in designing and optimising aircraft and jet engine configurations and performance. CFD has revolutionised airfoil design by its ability to optimise airfoil shapes to specified requirements. Key to predicting effects such as drag or the reversal of flow is accounting for the viscous effects in the airfoil near-wall region. The latter is commonly referred to as the boundary layer.

Drag prediction is important in the aerospace industry for economic reasons since it influences fuel burn costs (Anderson, 2007). The boundary layer region is typically described via the direct discretisation and solution of Navier-Stokes equations. When employing this approach, however, the boundary layer typically requires the largest part of computational resources, owing to the need for small mesh spacing normal to the boundary. In addition, the need for highly stretched elements on the boundary makes the process of meshing more specialised and time-consuming. Boundary layer approaches, on the other hand, have been demonstrated to quantify boundary layer effects in a far more efficient manner, and yet have received comparatively little attention since the 1980s.

Boundary layer approaches follow from the flow characteristics specific to many aerospace applications. The small thickness of the boundary layer prevalent in external high Reynolds number (small viscosity) attached flows, for example, permits certain approximations for governing equations within the boundary. Firstly, the variation of the pressure normal to the wall is negligibly small. Secondly, the variation of velocity along the wall is much smaller than the variation of velocity normal to the wall. These observations allow empirical relations to be employed to analytically integrate through the thickness of the boundary layer in a manner that reduces the dimensionality of the problem, vastly decreasing the computational resources consumed.

In industrial boundary layer modelling, the flow is divided into two regions: an inviscid flow region, where the flow is determined from models such as the Euler or full potential equations, and a viscid region, where flow is described by the boundary layer equations. This approach is computationally considerably more efficient than resolving the Navier-Stokes equations throughout, and various researches have demonstrated the efficiency of this approach.

Riziotis and Voutsinas (2008), for example, improved prediction of aerodynamic performance in dynamic stall conditions of airfoils. Jie and Zhou (2007) modelled transonic flow over complex three-dimensional aircraft configurations. Sekar and Laschka (2005) determined minimum flutter speed in transonic flows, Szmelter (2001) optimised transonic wings, Florea, Hall and Cizmas (1998) modelled cases of unsteady viscous separated flow through subsonic compressors and Soize (1992) modelled unsteady compressible flow in cascade blades at positive incidences.

However, a few difficulties are present with viscid-inviscid interaction schemes, for example, the so-called 'strong interaction problem'. Strong interactions exist, for example, in the trailing edge and separation regions where neither the viscous nor the inviscid flow is dominant locally. It is in these cases that the so-called 'Goldstein singularity' exists and where numerical interaction between the viscous and inviscid flow can fail or lack robustness (Katz and Plotkin, 2001). One way to overcome the Goldstein singularity is to solve the viscous and

inviscid flow regions simultaneously (Drela, 1985). However, this is computationally expensive and effectively limits one to using a potential flow scheme for the inviscid flow solution. Other existing interactive methods include the semi-inverse method of Le Balleur (1977), (1978), (1983) and Carter (1979), and the quasi-simultaneous method of Veldman (1979), (1980), (1981), (1984), (2001), (2005), (2009). Another important aspect when coupling the viscous and inviscid flow regions is that the inviscid solution needs to be informed of the boundary layer displacement. This is usually achieved by using a transpiration condition at the interface between the two flow regions, whereby a fictitious velocity is induced into the boundary layer to simulate its effect. The drawback of this scheme, however, is that it does not strictly conserve mass.

The objective of this study is to develop a method of solving boundary layer flow coupled to inviscid outer flow which counters the difficulties described above. In order to achieve this, we combine the following ingredients:

- An interactive solution technique to achieve computational efficiency and scaling for large problem sizes, as well as modularity of inviscid and boundary layer solvers.
- The use of a fully mass-conserving boundary condition, instead of the transpiration velocity condition.
- A coupling algorithm which circumvents the Goldstein singularity without the need for a monolithic simultaneous solution of both inviscid as well as viscous regions.

The algorithm developed will be used with an existing computational fluid dynamics solver to compute the influence of the boundary layer on the outer flow.

2. Mathematical formulation

2.1. Governing equations for out-of-boundary layer region

For the purposes of this work, we consider the incompressible (low Mach number) Navier-Stokes equations by which to describe the out-of-boundary layer flow, with the inviscid flow approximation:

Continuity

$$\frac{\partial}{\partial x_j} \rho u_j = 0 \tag{1}$$

Conservation of momentum (Newton's second law)

$$\frac{\partial}{\partial t}(\rho u_i) + \frac{\partial}{\partial x_j}(\rho u_i u_j) + \frac{\partial p}{\partial x_i} = \rho f_i + \frac{\partial}{\partial x_j}\left[\mu\left(\frac{\partial u_i}{\partial x_j} + \frac{\partial u_j}{\partial x_i} - \frac{2}{3}\frac{\partial u_k}{\partial x_k}\delta_{ij}\right)\right] \tag{2}$$

Where p is pressure, f is the body force, u is the velocity, ρ is density and μ is the dynamic viscosity.

2.2. Boundary layer model

The boundary layer equations employed in this work are those derived by Drela (Drela, 1985). Drela derived the momentum integral equation in terms of momentum and displacement thickness. These equations are known as the two-equation integral formulation based on dissipation closure for both laminar and turbulent flows, which eliminate the direct link between the profile shape and the pressure gradient, making them suitable for flow with strong interaction. The resulting two equations read:

$$\frac{d\theta}{d\xi} + \left(2 + H - M_e^2\right)\frac{\theta}{U_e}\frac{dU_e}{d\xi} = \frac{C_f}{2} \tag{3}$$

$$\theta\frac{dH^*}{d\xi} + \left[2H^{**} + H^*(1-H)\right]\frac{\theta}{U_e}\frac{dU_e}{d\xi} = 2C_D - H^*\frac{C_f}{2} \tag{4}$$

where θ is the momentum thickness, M_e the Mach number of the external flow, U_e the velocity of the external flow, C_f the skin friction coefficient, C_D the dissipation coefficient and ξ the coordinate parallel to the boundary layer. These equations also contain three different shape parameters: the shape parameter H, the energy thickness shape parameter, H^*, which eliminates the direct link between the H and the local external velocity U_e, and the density thickness shape factor H^{**}.

The shape parameters are defined as follows:

$$H = \frac{\delta^*}{\theta} \qquad H^* = \frac{\theta^*}{\theta} \qquad H^{**} = \frac{\delta^{**}}{\theta} \tag{5}$$

The momentum and displacement thicknesses θ and δ^* and the kinetic energy and density thickness θ^* and δ^{**} are defined as follows:

$$\theta = \int_0^\infty \left(1 - \frac{u}{U_e}\right) \frac{\rho u}{\rho U_e} d\eta \tag{6}$$

$$\delta^* = \int_0^\infty \left(1 - \frac{\rho u}{\rho U_e}\right) d\eta \tag{7}$$

$$\theta^* = \int_0^\infty \left(1 - \left(\frac{u}{U_e}\right)^2\right) \frac{\rho u}{\rho U_e} d\eta \tag{8}$$

$$\delta^{**} = \int_0^\infty \left(1 - \frac{\rho}{\rho_e}\right) \frac{u}{U_e} d\eta \tag{9}$$

where η is the similarity coordinate. The dissipation coefficient C_D and the skin friction coefficient C_f are defined as:

$$C_D = \frac{1}{\rho_e U_e^3} \int_0^\infty \tau \frac{\partial u}{\partial \eta} d\eta \tag{10}$$

$$C_f = \frac{2}{\rho_e U_e^2} \tau_w \tag{11}$$

The two dependent variables are defined as momentum and displacement thickness, θ and δ^*. U_e and M_e relate to the external inviscid flow and therefore do not represent additional unknowns. The undefined variables that remain are C_f, C_D, H^* and H^{**} for which the proposed functional dependencies by Drela and Giles (1987) are assumed:

$$H^* = H^*\left(H_k, M_e, \mathrm{Re}_\theta\right)$$
$$H^{**} = H^{**}\left(H_k, M_e\right)$$
$$C_f = C_f\left(H_k, M_e, \mathrm{Re}_\theta\right)$$
$$C_D = C_D\left(H_k, M_e, \mathrm{Re}_\theta\right)$$

In the above relations, H_k is the kinematic shape parameter defined with density taken as constant across the boundary layer and solely depends on the velocity profile and not the density profile. Since compressible and incompressible velocity profiles have closely similar shapes, the above correlations are based on the kinematic shape parameter for compressible flow cases (Drela, 1985).

H_k was developed as an empirical expression by Whitfield (1978) in terms of the conventional shape parameter and edge Mach number M_e as follows:

$$H_k \equiv \frac{\int_0^\infty \left(1 - \frac{u}{U_e}\right) d\eta}{\int_0^\infty \left(1 - \frac{u}{U_e}\right) \frac{u}{U_e} d\eta} = \frac{H - 0.29 M_e^2}{1 + 0.113 M_e^2} \tag{12}$$

Laminar closure equations empirically derived from the Falkner-Skan profile family are as follows (Drela, 1985):

The energy thickness shape parameter equations:

$$H^* = 1.515 + 0.076 \frac{(4 - H_k)^2}{H_k}, H_k < 4$$

$$H^* = 1.515 + 0.04 \frac{(H_k - 4)^2}{H_k}, H_k > 4 \tag{13}$$

The skin friction coefficient:

$$\mathrm{Re}_\theta \frac{C_f}{2} = -0.067 + 0.01977 \frac{(7.4 - H_k)^2}{H_k - 1}, H_k < 7.4$$

$$\mathrm{Re}_\theta \frac{C_f}{2} = -0.067 + 0.022 \left(1 - \frac{1.4}{H_k - 6}\right)^2, H_k > 7.4 \tag{14}$$

The dissipation coefficient:

$$\mathrm{Re}_\theta \frac{2C_D}{H^*} = 0.207 + 0.00205(4 - H_k)^{5.5}, H_k < 4$$

$$\mathrm{Re}_\theta \frac{2C_D}{H^*} = 0.207 - 0.003 \frac{(H_k - 4)^2}{(1 + 0.02(H_k - 4)^2)}, H_k > 4 \tag{15}$$

The density thickness H^{**} was derived by Whitfield (1978) and is defined as follows:

$$H^{**} = \left(\frac{0.064}{H_k - 0.8} + 0.251\right) M_e^2 \tag{16}$$

Note that this shape parameter is negligible for low subsonic flows and has only a small effect on transonic flows.

The laminar closure equations reach a singularity at the point where H_k reaches 4, which is where the function (13) reaches a minimum. This is referred to as the 'Goldstein singularity' at a boundary layer separation point. The vanishing derivative of H^* causes a singularity in equation (4), which can only be avoided if U_e adjusts to cause the rest of the equation to tend to zero as well. Therefore, any boundary layer method with a prescribed U_e that reaches separation will fail at this point.

Various methods have been proposed to circumvent this problem. Firstly, the inviscid flow and boundary layer equations may be solved simultaneously (Drela, 1985). Secondly, in the semi-inverse method of Le Balleur (1977) and Carter (1979), the boundary layer is solved in reverse, i.e. for a given displacement thickness, the velocity distribution at the edge of the boundary layer is computed. By then comparing this computed velocity with the target distribution imposed by the inviscid flow, a relaxation formula is used to obtain a new estimate for displacement thickness. Thirdly, using the quasi-simultaneous approach of Veldman (1979), a simplified model for the inviscid flow is solved simultaneously with the boundary layer thickness to circumvent the singularity. While this yields only an approximate solution to the full system, the true solution can then be obtained through iterative refinement. Simultaneous solution of the entire system may be computationally costly, while the quasi-simultaneous method has been shown to outperform the semi-inverse method in terms of convergence speed (Lock and Williams, 1987). In this paper, therefore, the approach we propose is based on the quasi-simultaneous philosophy.

In the quasi-simultaneous approach, the simplified inviscid flow model is obtained by retaining only principal diagonals in the external flow operator which maps the displacement thickness at the boundary points to the edge velocities at those points (Veldman, 2009). Thus, only the influence of a limited neighbourhood of points is taken into account as the boundary layer adjusts, depending on how many diagonals are retained. In this work, we propose an alternative approach. To avoid prescribing the velocity directly, for the purposes of the boundary layer solution, the outer inviscid flow is assumed to be confined to a notional two-dimensional channel. This channel has a fixed specified total volume flow rate $\dot{V}$ and a varying specific height $h(x_1)$ which is calculated to reproduce the desired velocity profile given an estimated boundary layer thickness (Drela, 2010). The velocity is then solved using the

channel model together with the boundary layer equations, allowing the singularity to be avoided. Repeating the process by feeding back the newly calculated displacement thickness as the updated estimate, the process can be iterated until convergence is reached. Although $\dot{V}$ is an arbitrary value (since $h(x_1)$ is calculated to always give the desired velocity profile) it plays a role in the accuracy versus stability trade-off, smaller values yielding a more stable solution but requiring more iterations to reach convergence to an accurate solution.

Accordingly, the velocity is written as:

$$U_e(\xi) = \dot{V} \big/ \big(h(\xi) - \delta^*(\xi) \big). \tag{17}$$

Here $h(x_1)$, the specific channel height, is calculated from the specified velocity by

$$h(\xi) = \dot{V} \big/ U_{e,spec}(\xi) + \delta^*_{estimate}(\xi) \tag{18}$$

Where $\delta^*_{estimate}(\xi)$ is an estimated displacement thickness and $U_{e,spec}$ is the velocity obtained from the inviscid solution.

It is unavoidable that the final U_e will differ slightly from $U_{e,spec}$, although the more accurate is $\delta^*_{estimate}(\xi)$, the smaller this difference will be. The greater the value of $\dot{V}$, the closer U_e will be to $U_{e,spec}$, but if it is set too high, the Goldstein singularity is approached once again as the influence of $\delta^*(\xi)$ on U_e is lessened.

Equation (17) becomes an additional equation to solve along with equations (3) and (4). This allows the simultaneous solution of displacement thickness and velocity, circumventing the singularity, while avoiding the need to solve the entire viscous and inviscid flow domains simultaneously.

3. Solution procedure

3.1. Inviscid flow

In this investigation, we restrict ourselves to incompressible outer flow. The flow solver is based on the artificial compressibility characteristic-based split (CBS-AC) scheme (Nithiarasu, 2003, Malan and Lewis, 2011). The three steps of the CBS-AC algorithm can be written as:

Step 1: Intermediate momentum

$$\Delta(\rho u_i)^* = \Delta t \left[-\frac{\partial}{\partial x_j}(\rho u_i u_j) + \frac{1}{Re}\frac{\partial \tau_{ij}}{\partial x_j} + \frac{\Delta t}{2} u_k \frac{\partial}{\partial x_k}\left(\frac{\partial}{\partial x_j}(\rho u_i u_j) \right) \right]^n \tag{19}$$

where the asterisk indicates an intermediate quantity. Viscous terms are included although they are negligible for inviscid flow and the flow solver is not required to resolve the boundary layer.

Step 2: Density or pressure

$$\left(\frac{1}{c^2}\right)^n \Delta p = \left(\frac{1}{c^2}\right)^n (p^{n+1} - p^n) = -\Delta t \left[\frac{\partial(\rho u_i)}{\partial x_i} + \theta_1 \frac{\partial \Delta(\rho u_i)^*}{\partial x_i} - \Delta t \theta_1 \left(\frac{\partial^2 p^n}{\partial x_i \partial x_i} + \theta_2 \frac{\partial^2 \Delta p}{\partial x_i \partial x_i} \right) \right] \tag{20}$$

where n denotes the previous pseudo (iteration) time-step and $n+1$ is the new iteration being solved for.

Step 3: Momentum correction

$$\Delta(\rho u_i) = \rho u_i^{n+1} - \rho u_i^n = \Delta(\rho u_i)^* - \Delta t \frac{\partial p^{n+\theta_2}}{\partial x_i} \tag{21}$$

Where $0.5 \le \theta_1 \le 1$ and $0 \le \theta_2 \le 1$. For the explicit artificial-compressibility scheme employed, $\theta_2 = 0$ is used. The artificial compressibility formulation allows for a finite value of c^2 to be used for incompressible flows, calculated as per Malan *et al.* (2002).

3.2. Boundary layer solution

To ensure numerical stability, the Crank-Nicolson differencing scheme is used to discretise the boundary layer equations as represented by equations (3) and (4), along with the auxiliary velocity equation (17).

The momentum equation (3) is discretised as:

$$f_1 \equiv \frac{\theta_n - \theta_{n-1}}{\Delta\xi_n} + \left(2 + H_{n-\frac{1}{2}}\right)\frac{\theta_{n-\frac{1}{2}}}{U_{e,n-\frac{1}{2}}}\frac{U_{e,n} - U_{e,n-1}}{\Delta\xi_n} - \frac{C_{f,n-\frac{1}{2}}}{2} = 0 \tag{22}$$

where for the purpose of the boundary layer equations, n denotes a node number. Further, $C_f = C_f(H_k, Re)$ as given by (14) and $n - \frac{1}{2}$ refers to an average value between node n and $n - 1$, for example, $\theta_{n-\frac{1}{2}} = \frac{1}{2}\theta_n + \frac{1}{2}\theta_{n-1}$.

The shape parameter equation (4) is discretised as:

$$f_2 \equiv \theta_{n-\frac{1}{2}}\frac{H_n^* - H_{n-1}^*}{\Delta\xi_n} - 2C_{D,n-\frac{1}{2}} + H_{n-\frac{1}{2}}^*\frac{C_{f,n-\frac{1}{2}}}{2} + H_{n-\frac{1}{2}}^*\left(1 - H_{n-\frac{1}{2}}\right)\frac{\theta_{n-\frac{1}{2}}}{U_{e,n-\frac{1}{2}}}\frac{U_{e,n} - U_{e,n-1}}{\Delta\xi_n} = 0 \tag{23}$$

where $C_f = C_f(H_k, Re)$ as given by (14) and $C_d = C_d(H_k, Re)$ as given by (15). To simplify the working, we shall now restrict ourselves to incompressible flow, with the result that $H_k = H = \delta^*/\theta$ and $H^{**} = 0$.

The auxiliary velocity equation (17) is discretised as:

$$f_3 \equiv \frac{\dot{V}}{\left(h_n - \delta_n^*\right)} - U_{e,n} = 0 \tag{24}$$

The equations (22-24) are now solved as an initial value problem using a point-by-point local Newton method. That is, given initial values for δ_0, θ_0, and $U_{e,0}$, the system of three equations

$$f_i(\delta_n^*, \theta_n, U_{e,n}) = 0 \qquad \text{where } i = 1,2,3 \tag{26}$$

is solved first for $n = 1$, then $n = 2$ and so on. The 3×3 Jacobian $\dfrac{\partial(f_1, f_2, f_3)}{\partial(\delta_n^*, \theta_n, U_{e,n})}$ is calculated analytically at each point n using the exact discretised governing equations. The initial values used to start the Newton iterations are taken as the values from the previous point.

3.3. Initial condition

Initial values δ_0^* and θ_0 are needed and the logical choice of zero cannot be used for the Crank-Nicolson method since C_f and C_D are singular there. Therefore, the initial increment is instead solved using the similarity solution of Blasius, to give

$$\delta_1^* = 1.7208\sqrt{\frac{\nu\Delta\xi_1}{U_e}} \quad \text{and} \tag{26}$$

$$\theta_1 = 0.664\sqrt{\frac{\nu\Delta\xi_1}{U_e}}. \tag{27}$$

The initial values obtained from this function are a sufficiently close approximation to solve most boundary layer solutions (Drela, 1985). The boundary layer equations are then solved from the second point onwards.

The initial value for U_e is set at $U_{e,spec}$, which is obtained from the inviscid solver. To improve robustness the velocity function (17) is only activated as the singularity is approached; i.e. U_e is set equal to $U_{e,spec}$ for $H < 2.5$ after which the velocity equation (17) is used to solve for U_e.

3.4. Mesh movement

The mesh movement routine is a simple interpolation function   (Oxtoby and Malan, 2012)

$$\boldsymbol{\delta} = r\boldsymbol{\delta}_1 + (1-r)\boldsymbol{\delta}_2 \tag{28}$$

where

$$r = \frac{d_2^{3/2}}{\left(d_1^{3/2} + d_2^{3/2}\right)} \tag{29}$$

In this case $\boldsymbol{\delta}$ is the displacement of the grid point from its original position, d_1 and d_2 are the shortest distances from that point to the internal and external boundaries respectively, and $\boldsymbol{\delta}_1$ and $\boldsymbol{\delta}_2$ are the displacements of those two closest boundary points. Though this approach is somewhat simplistic, it is sufficient for small displacements in aerodynamic applications and is selected for its negligible computational cost.

3.5. Coupling and interaction method

The interaction method between the solver and the different routines to calculate the boundary and move the mesh happens as follows:

- Firstly, the solver lets the flow solution converge to a point where the residual is less than the specified tolerance. Both boundary layer and inviscid regions are solved concurrently.
- Secondly, the solver moves the boundary nodes to the position of a streamline at the boundary surface. This is determined by the displacement thickness δ^* calculated by the boundary layer routine. Hence, boundary node n is displaced as follows:

$$\delta\mathbf{x}_n^{(i)} = \alpha\delta_n^*\mathbf{n} + (1-\alpha)\delta\mathbf{x}_n^{(i-1)} \tag{30}$$

  where $\delta\mathbf{x}_n^{(i)}$ and $\delta\mathbf{x}_n^{(i-1)}$ are the new and previous displacements of node n from its original position, δ^* is the computed boundary layer thickness, $\mathbf{n}$ is a unit vector normal to the boundary and α is an under-relaxation coefficient between 0 and 1. Under-relaxation is necessary to stabilise the viscid-inviscid coupling process with the value selected as large as possible to produce a stable solution. For all the problems considered, a value of $\alpha = 0.1$ was found to be sufficient.
- Following the mesh movement step, the flow residual is calculated again. If this residual is less than the convergence tolerance, the program will give the resulting output, otherwise it restarts from the beginning, repeating the process.

3.6. Goldstein singularity

As described, the $\dot{V}$ parameter determines the tradeoff between robustness of the boundary layer solution and speed of convergence of the iterative process. The early cycles of computing the boundary layer around an airfoil are particularly prone to instability due to the large adverse pressure gradient near the trailing edge. $\dot{V}$ is therefore set to a conservative value of 0.005 to ensure robust solution. It was found that for the iterative process to converge, it had to be "frozen" at some stage. To achieve this, the maximum percentage change in δ^* over the entire boundary layer was monitored and when it fell below a set threshold, here set to 0.2%, $\delta^*_{estimate}$ was no longer updated.

3.7. Wake

The calculation of the boundary layer into the wake has not been included in this study, and instead an estimated function has been used for wake behind an airfoil. The function fitted approximately to data for a NACA0012 airfoil was:

$$\delta^*_{wake}(x_1) = 10^{A-3.2(x_1-1)} \tag{31}$$

where A must be selected so that $\delta^*_{wake}(1) = \delta^*(\xi_{te})$. The trailing edge is at $\xi = \xi_{te}$. Since this does not accurately portray the shape of the wake, the approximation function (31) will cause a sacrifice of accuracy in the displacement thickness results through and beyond the trailing edge into the wake. Accurate representation of the wake requires implementation of different correlations (Katz and Plotkin, 2001) but otherwise is essentially the same as the process followed for the boundary layer.

4. Results and discussion

For purposes of verification and validation, the proposed modelling technology was applied to a number of benchmark problems. This is discussed in the following paragraphs.

4.1. Flat and angled plates

The first test cases consisted of laminar flow over a flat plate. Finite difference meshes were employed, with mesh spacing as listed in Table 1. Figure 1 shows the two-integral numerical solution compared with the solution of the Blasius equations (Blasius, 1908) for a mesh spacing $\Delta\xi = 0.05$. Interaction with the inviscid flow is not considered in this initial test, with the external velocity set constant at 1 m.s^{-1}. The viscosity used in these test cases is 1×10^{-5} m^2.s^{-1} with Reynolds numbers going up to 4×10^5.
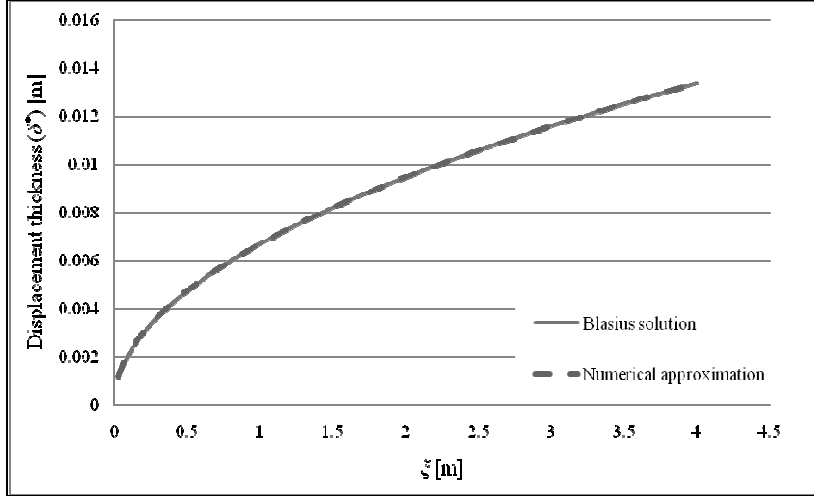
Figure 1: Comparison between analytical solution (Blasius) and the numerical solution.

To assess mesh convergence, we compute the average percentage error between the Blasius similarity solution and the two-integral solution as follows:

$$Error = \frac{1}{N}\sum_{n=1}^{N}\left|\delta^*_{n,similarity} - \delta^*_{n,computed}\right|\Big/\delta^*_{n,similarity} \tag{32}$$

Table 1 shows the errors resulting from various mesh spacings:

	Mesh spacing ($\Delta\xi$)	Error (%)
Case 1	0.267	42.46%
Case 2	0.05	2.06%
Case 3	0.0267	0.55%
Case 4	0.01	0.083%

Table 1: Comparison between different mesh sizes for a flat plate

These errors are plotted in Figure 2 as a function of mesh spacing. The slope of the log-log plot approaches 1.93, demonstrating the expected quadratic convergence rate of the Crank-Nicolson scheme.
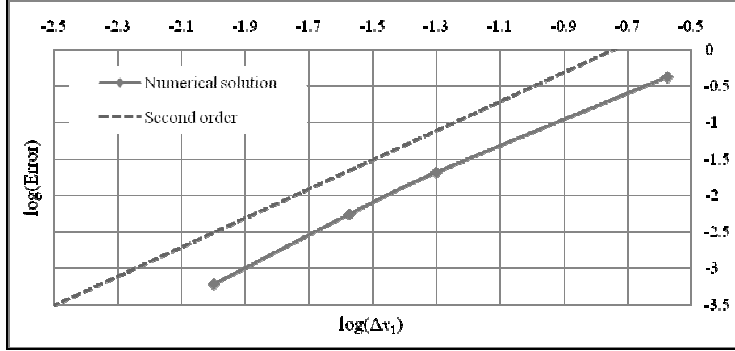
Figure 2: Convergence rate for the Blasius solution using different grid spacings, with the dashed line depicting formal second-order accuracy.

We now consider an inclined plate at an angle of $\pi\beta/2$ with respect to the oncoming airstream, as previously, finite difference meshes were employed. Table 2 summarises the resulting errors between the numerical boundary-layer solution and the Falkner-Skan similarity solution where again the outer velocity distribution is fixed as the inviscid analytical solution. The results again indicate quadratic convergence, reaching convergence rates of 2.09 and 1.83 in the two cases respectively.

	Step size ($\Delta\xi$)	Error (%)
$\beta = 0.3$	0.05	2.47%
	0.02	0.35%
	0.01	0.082%
$\beta = 0.4$	0.05	2.11%
	0.02	0.23%
	0.01	0.065%

Table 2: Comparison of different mesh sizes for angled plates.

We now allow the entire coupled system to solve for plates at various angles of inclination. The boundary conditions for these test cases were set to have a fixed velocity imposed on the outer boundary, namely the analytical solution of the velocity in the inviscid case, and unconstrained pressure. Since there is no "far-field" region in which velocity tends to a constant, the boundary conditions have a big influence on the solution. Therefore, to obtain a meaningful comparison with the similarity solution, it was necessary to specify them exactly.

The predicted magnified boundary layer displacement mesh for a flat plate is depicted in Figure 3. The structured mesh consists of 5 226 nodes with $\Delta x_1 = 0.02$ m and the solver converged to a solution with an error percentage of 0.2%. The solver was found to be stable and robust, with only two tuneable parameters to be set: the under-relaxation parameter α (see equation (31)), which affects the iterations between the inviscid and boundary layer solver, and the CFL number of the inviscid solver. In this case, α was set to 0.7, and the CFL number was set to 0.9. The solver was run in parallel on eight Intel Xeon CPUs of 2.33 GHz each and required 30.3 seconds to converge. Figure 4 compares the Falkner-Skan similarity solution and that of the interacting solver. The errors evaluated using equation (32) varied between 0.7% and 1.2% for the three cases shown.

Note however that the solutions should not agree precisely as the similarity solution assumes the inviscid velocity distribution (i.e. no influence of boundary layer displacement on the inviscid outer flow). The number of viscid-inviscid iterations required to converge the solution by a five-order of magnitude drop in residual was between 16 and 18 for these cases, with an under-relaxation coefficient of 0.9 used.
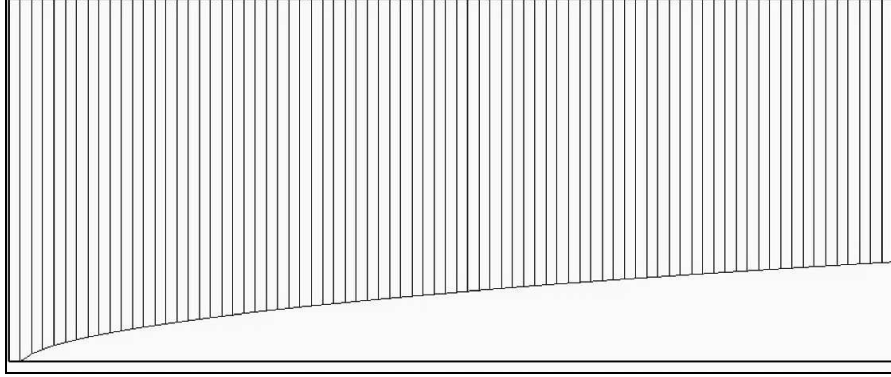
Figure 3: Boundary mesh movement of flat plate, magnified 200 times in the vertical direction.
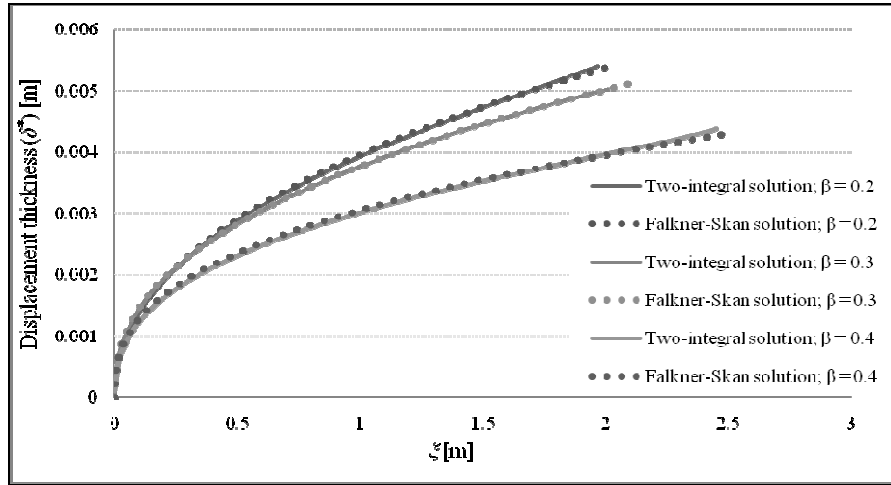

Figure 4: Comparison between the two-integral solution and that of Falkner-Skan.

4.2. NACA0012 airfoil

As a concluding example, the flow over a symmetrical airfoil (NACA0012) at zero angle of attack is calculated. Results obtained are compared with simulations of the same airfoil from XFOIL 6.9, a code developed by Drela and Youngren (2001), to validate the solution of the boundary layer code. A solution for a case of a laminar boundary layer is evaluated at Re = 10 000, to obtain the following results using an under-relaxation parameter of 0.1 and converging to a solution within 72 coupled iterations, with a drop in residual of five orders of magnitude. An unstructured computational mesh consisting of 12 064 nodes was employed for the inviscid fluid domain as shown in Figure 9.

Figure 5 shows the solution of the displacement thickness at different stages of convergence. A slight inaccuracy in the vicinity of the trailing edge is evident, where the maximum disparity between the codes of 13.2% occurs. The velocity equation (17) suggested overcomes the Goldstein singularity existing at the point of shear stress vanishing but a proper solution of the wake would be required to ensure accurate calculation of the displacement thickness into the wake, whereas in this work, a wake function was used to simulate the displacement thickness across the trailing edge into the wake. The average difference in predicted displacement thickness between the developed technology and that of XFOIL using equation (32), is 3.95%.

Snapshots were taken at certain stages throughout convergence to show how the boundary layer solution adjusts as the system converges. The results in Figure 5 are compared with those of XFOIL for this specific flow case. The line name "intermediate" refers to a point in convergence where there is a 10% difference between U_e and $U_{e,specified}$ at the final point. Figure 7 depicts the shape factor (H) during different stages of convergence. The shape factor begins at a value slightly lower than the Blasius value ($H = 2.59$) and grows gradually towards the trailing edge. Recall that the singularity occurs at $H = 4$.
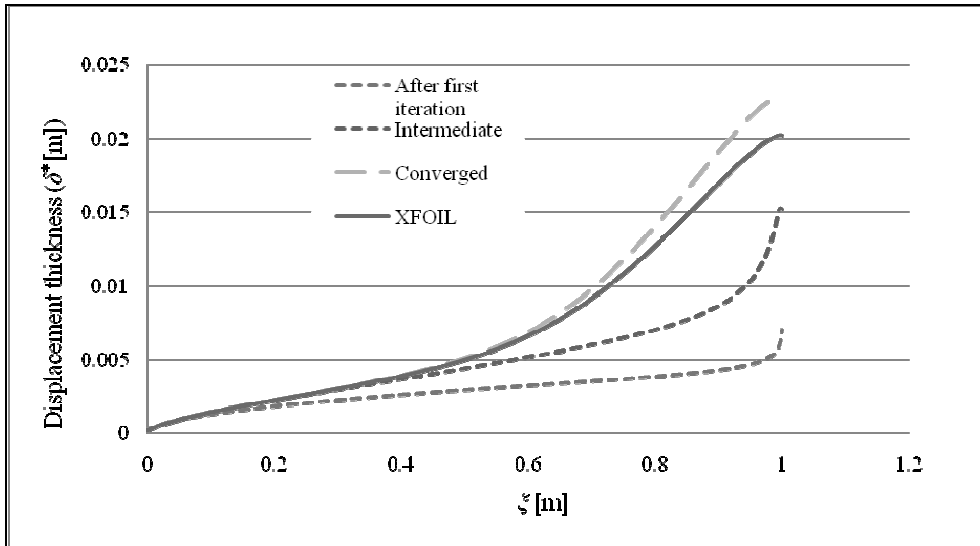
11

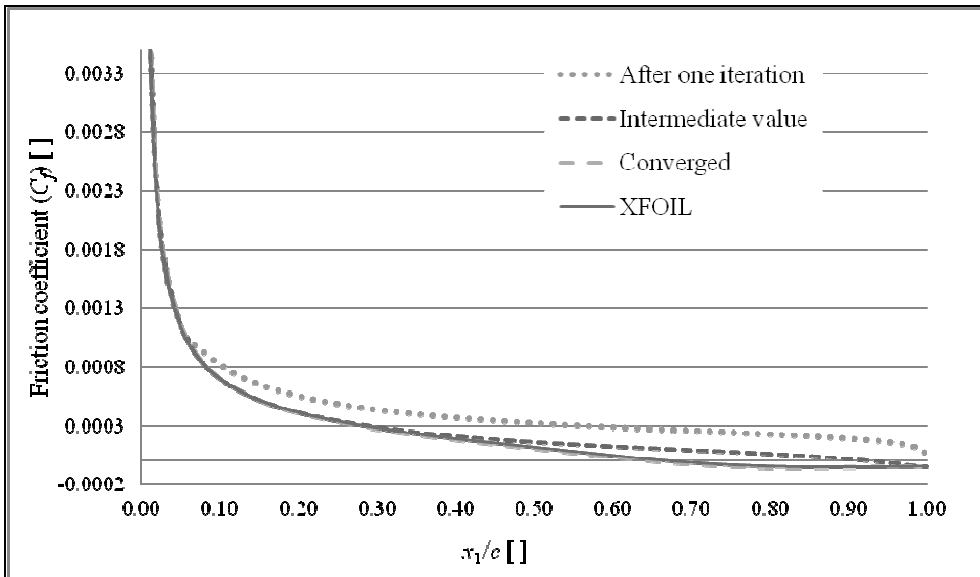**Figure 5: Comparison of displacement thickness at different stages of convergence for a NACA0012 airfoil.**

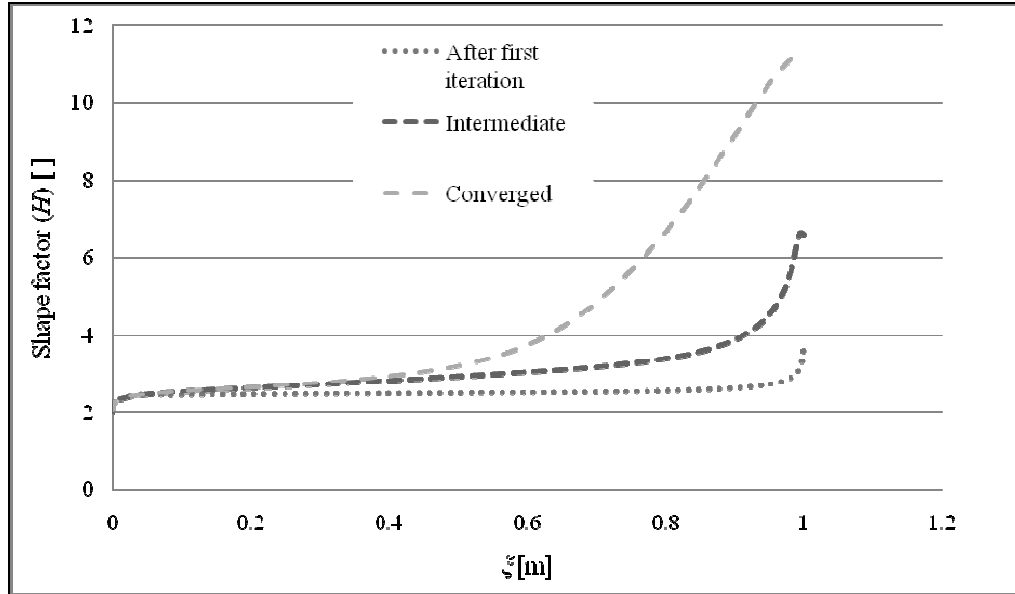**Figure 6: Skin friction coefficient at different stages of convergence.**

Figure 7: Shape factor at different stages of convergence.

Figure 7 depicts the friction coefficient (C_f) as calculated by equation (14) at different stages of convergence, compared with the XFOIL values for a NACA0012 airfoil. The friction coefficient is important since this dimensionless parameter relates to the friction drag found in the boundary layer. The smaller the friction drag, the more economical the fuel-usage of the aircraft. The C_f values converge to the XFOIL solution with an overall error of 4.7% and a maximum discrepancy of 7.7% to present an accurate value to use for estimating the overall effects of the drag.
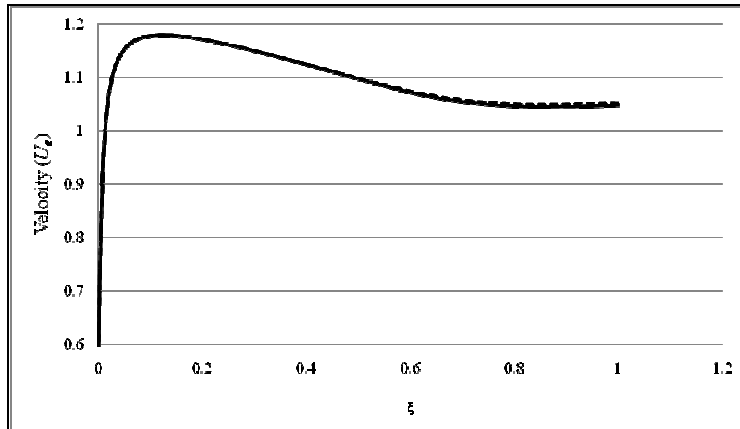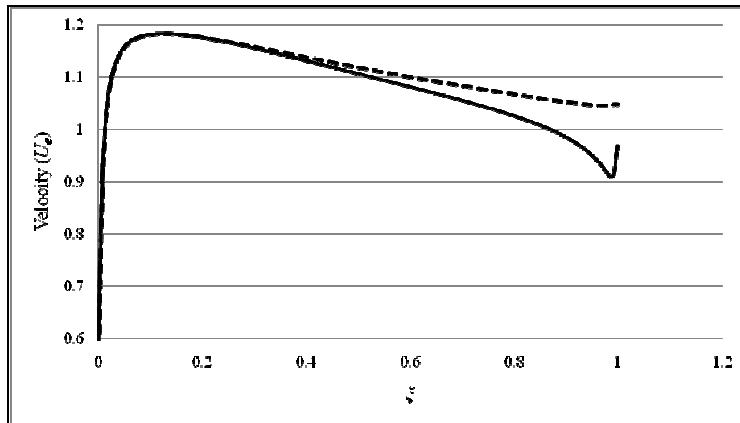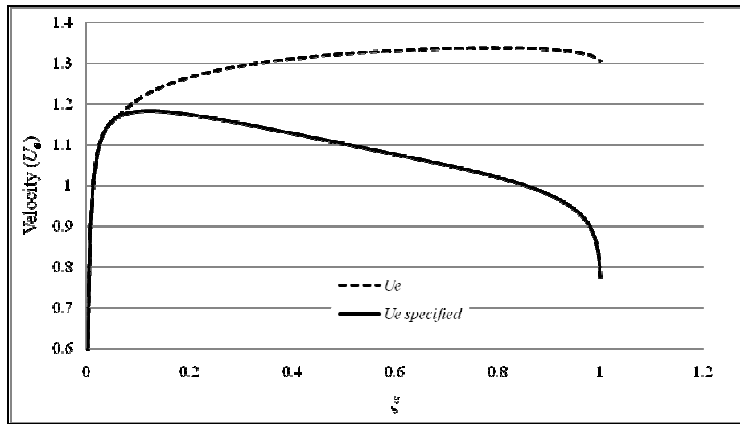
Figure 8: Comparison between the velocity imposed by inviscid solution and that obtained from the boundary layer solution, after first iteration (top), intermediate (middle) and converged (bottom).
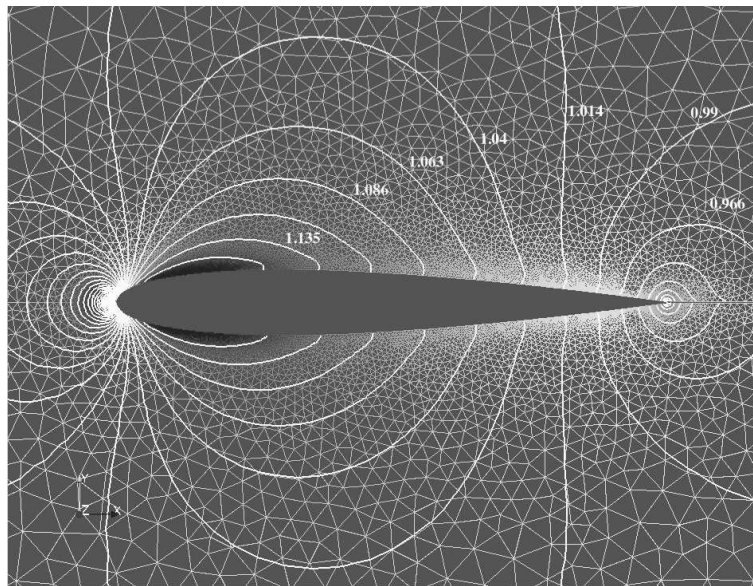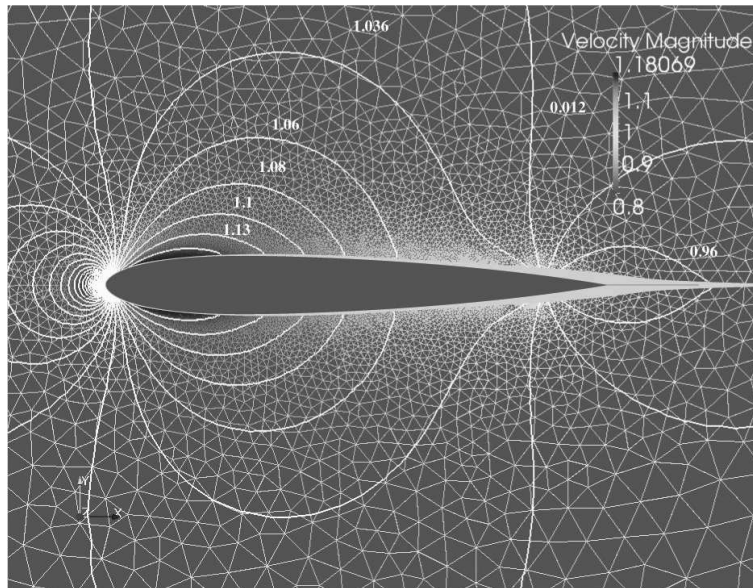
14

Figure 9: Mesh and velocity contours around the NACA0012 airfoil: Viscous flow (top) and inviscid flow (bottom). Velocity distribution in m.s⁻¹.
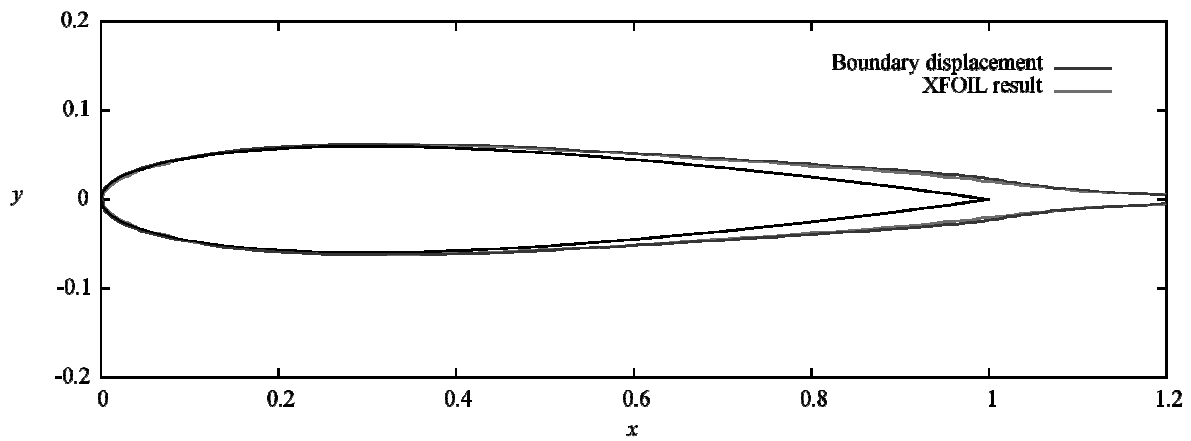

Figure 10: Mesh movement around the NACA0012 airfoil.

Figure 8 shows the velocity that is computed by the auxiliary boundary layer equation (17) (in order to avoid the Goldstein singularity) compared with the velocity specified from the inviscid solver. It is compared at the different

15

stages of convergence, showing that the two velocities converge. Figure 9 shows the unstructured mesh with velocity contours around the NACA0012 airfoil for both the viscous and inviscid flow cases. The viscous case also shows the mesh movement depicted by the light grey area around the airfoil. Finally, Figure 10 displays the boundary layer thickness around the airfoil compared with the result obtained from XFOIL. It is evident that as the solver reaches the trailing edge and moves into the wake, there is a loss in accuracy. This is due to the assumed wake function as discussed in Section 3.7.

5. Conclusion

Generally, in the aeronautics industry, boundary layer effects are solved using the Navier-Stokes equations, which are computationally very expensive. The boundary layer is not only important to determine appropriate shapes to minimise drag across a body and thereby save fuel costs or to avoid separation but also to simulate flow through blade cascades in compressors and turbines.

A novel viscous-inviscid modelling technology was developed, whereby the viscous region was described by boundary layer equations while the outer region was solved via an incompressible flow solver. In the case of the viscous boundary layer region, the two-integral method of Drela (1985) was used, obtaining the momentum integral equation in terms of momentum and displacement thickness, to solve flow in the boundary layer and predict the displacement thickness. The boundary layer equations were then discretised using the Crank-Nicolson differencing scheme (second-order implicit scheme) to ensure stability. These equations were solved point by point as an initial value problem by a local Newton method, since this method is relatively fast to converge, if the initial approximation is close to the solution. The method is able to solve past the separation singularity (Goldstein singularity) by using a quasi-simultaneous method with an auxiliary velocity equation suggested by Drela (2010). A coupling algorithm based on mesh-movement is used to account for the boundary layer thickness. Moving the mesh is considered more accurate and applicable to generic solvers than solving for an additional transpiration condition, which introduces spurious mass into the system. This allows for iterative solution of inviscid and boundary layer regions.

The developed modelling technology is thoroughly validated in terms of accuracy and robustness via application to a number of test cases. Two classes of test cases were considered: one with only the boundary layer solver and the other with the viscous-inviscid coupling between the boundary layer solver and an existing inviscid solver. The first class of boundary layer cases consisted of flow over a flat plate as well as flow over an inclined plate at different angles of attack. The second class of test cases involved the same problems, in addition to the flow over a NACA0012 airfoil (results for the latter were compared with those of the XFOIL program). The developed boundary layer modelling scheme was proved second-order accurate. In both cases, the solvers proved to be robust and stable and only tuneable for the sake of convergence by the under-relaxation parameter and the CFL number.

The methodology can be extended in a straightforward manner to treat practical airfoil design problems with transition to turbulent flows and mild flow separation by adding the additional parameters and equations given in the work of Drela (1985). Further, to increase the accuracy of the interactive method the proper closure equations for the wake should be solved as suggested by Drela (1985). The inviscid solver is a separate module in this study, which has the potential to be extended to transonic compressible flow.

References

Anderson, D.A. 2007. *Fundamentals of aerodynamics.* 4th ed. New York: McGraw-Hill.

Blasius, H. 1908. The boundary layers in fluids with little friction. *National Advisory committee for Aeronautic,* Technical memorandum1256. Washington.

Carter, J.E. 1979. A new boundary layer inviscid iteration technique for separated flow. *American Institute of Aeronautics and Astronautics.* Paper 1979 – 1450.

Cebeci, T. & Cousteix, J. 2005. *Modelling and computation of boundary layer flows.* Los Angeles, CA: Horizon.

Drela, M. 1985. *Two-dimensional transonic aerodynamic design and analysis using the Euler equations.* PhD thesis. Cambridge, MA: Department of Aeronautics and Astronautics. Massachusetts Institute of Technology.

Drela M. 2010. *Private communication.*

Drela, M. & Giles, M.B. 1987. Viscous-inviscid analysis of transonic and low Reynolds number airfoils. *American Institute of Aeronautics and Astronautics Journal,* 25(10):347 – 1355.

Drela, M. & Youngren, H. 2001. *XFOIL 6.9 User Primer.* Cambridge, MA: Department of Aeronautics and Astronautics. Massachusetts Institute of Technology.

Florea, R., Hall, K.C. & Cizmas, P.G.A. 1998. Reduced-order modelling of unsteady viscous flow in a compressor cascade. *American Institute of Aeronautics and Astronautics Journal*, 36(6):1039 – 1048.

Jie, L. & Zhou, Z. 2007. A structured mesh Euler and interactive boundary layer method for wing/body configurations. *Chinese Journal of Aeronautics*, 21:19 – 27.

Katz, J. & Plotkin, A. 2001. *Low speed aerodynamic.* 2nd ed. New York: Cambridge University Press.

Le Balleur, J.C. 1977. Viscous-inviscid flow matching: Analysis of the problem including separation and shock waves. *La Recherche A´erospatiale*, 6:349 – 358.

Le Balleur, J.C. 1978. Couplage visqueux non-visqueux: M´ethode num´erique et applications aux ´ecoulements bidimensionnels transsoniques et supersoniques. *La Recherche A´erospatiale*, 2:65 – 76.

Le Balleur, J.C. 1983. Numerical viscous-inviscid interaction in steady and unsteady flows. *Proceedings of the Second Symposium, Numerical and Physical Aspects of Aerodynamic Flow,* 259 – 284.

Lock, R. & Williams, B. 1987. Viscous-inviscid interactions in external aerodynamics. *Progress Aerospace Science*, 24:51 – 171.

Malan, A.G. & Lewis, R.W. 2011. An artificial compressibility CBS method for modelling heat transfer and fluid flow in heterogeneous porous materials. *International Journal for Numerical Methods in Engineering*, 86(7), In press.

Malan, A.G., Lewis, R.W. & Nithiarasu, P. 2002. An improved unsteady, artificial compressibility, finite volume scheme for viscous incompressible flows: Part I. Theory and Implementation. *International Journal for Numerical Methods in Engineering*, 54(5):695 – 714.

Nithiarasu, P. 2003. An efficient artificial compressibility (AC) scheme based on the characteristics based split (CBS) method for incompressible flows. *International Journal for Numerical Methods in Engineering*, 56:1815 – 1845.

Oxtoby, O.F. & Malan, A.G. 2012. A matrix-free, implicit, incompressible fractional-step algorithm for fluid-structure interaction applications. *Journal of Computational Physics, http://dx.doi.org/10.1016/j.jcp.2012.04.037.* In press.

Riziotis, V.A. & Voutsinas, S.G. 2008. Dynamic stall modelling on airfoils based on strong viscous-inviscid interaction coupling. *International Journal of Numerical Methods in Fluids*, 56:185 – 208.

Sekar, W.K. & Laschka, B. 2005. Calculation of the transonic dip of airfoils using viscous-inviscid aerodynamic interaction method. *Aerospace Science and Technology*, 9:661 – 671.

Soize, C. 1992. Strong coupling between inviscid fluid and boundary layer for airfoils with a sharp edge. II. 2D unsteady case for isolated airfoil and straight blade cascade. *La Recherche Aerospatiale*, 3:23 –53.

Szmelter, J. 2001. Multipoint Aerodynamic wing optimisation in viscous flow. *Journal of Aircraft*, 38(5):860 – 867.

Veldman, A.E.P. 1979. A numerical method for the calculation of laminar incompressible boundary layers with strong viscous-inviscid interaction. *Report NLR TR 79023.* Netherlands:National Aerospace Laboratory.

Veldman, A.E.P. 1980. Boundary layers with strong interaction: From asymptotic theory to calculation method. *Conference on Boundary and Interior Layers: Computational and Asymptotic Methods.* Dublin.

Veldman, A.E.P. 1981. New, quasi-simultaneous method to calculate interacting boundary layers. *American Institute of Aeronautics and Astronautics Journal*, 19:79 – 85.

Veldman, A.E.P. 1984. A numerical view on strong viscous-invisicid interaction. In: WG Habashi (ed.) *Computational Methods in Viscous Flows.* Southampton: Pineridge Press.

Veldman, A.E.P. 2001. Matched asymptotic expansions and the numerical treatment of viscous-inviscid interaction. *Journal of Engineering Mathematics*, 39:189 – 206.

Veldman, A.E.P. 2005. Quasi-simultaneous viscous-inviscid interaction for transonic airfoil flow. *4th American Institute of Aeronautics and Astronautics Theoretical Fluid Mechanics Meeting.* AIAA 2005-4801. Toronto.

Veldman, A.E.P. 2009. A simple interaction law for viscous-inviscid interaction. *Journal of Engineering Mathematics*, 65:367 – 383.

White, F.M. 2006. *Viscous fluid flow.* 3rd ed. Singapore: McGraw-Hill.

Whitfield, D.L. 1978. Analytical description of the complete turbulent boundary layer velocity profile. *American Institute of Aeronautics and Astronautics Papers 78-1158.* 11th Fluid and Plasma Dynamics Conference. (July):12.